



Influence of magnetohydrodynamics and heat transfer on the reverse roll coating of a Jeffrey fluid: A theoretical study

Journal of Plastic Film & Sheeting
2022, Vol. 38(1) 72–104
© The Author(s) 2021
Article reuse guidelines:
sagepub.com/journals-permissions
DOI: 10.1177/87560879211029693
journals.sagepub.com/home/jpf
 SAGE

Fateh Ali¹ , Yanren Hou¹,
Muhammad Zahid² , MA Rana³ and
Muhammad Usman¹

Abstract

The purpose of this article is to provide a mathematical model of magnetohydrodynamic (MHD) non-isothermal flow of an incompressible Jeffrey fluid as it goes through a minimal gap between the two counter rotating rolls. The dimensionless forms of governing equations are obtained by using appropriate dimensionless parameters. The LAT (lubrication approximation theory) is utilized to simplify the dimensionless form of governing equations. Analytical solutions for the velocity, pressure gradient, flow rate, Nusselt number and temperature distribution are presented. How the Jeffrey parameters, MHD and velocities ratio influence on the flow patterns and heat transfer rate are explored. Outcomes of some significant engineering quantities such as flow rate, power input, pressure distribution and roll separation force are obtained numerically in tabular form and some are displayed graphically. We found that the MHD parameter served as a controlling parameter for different engineering quantities like velocity, temperature, flow rate, and coating thickness. Moreover, the coating thickness on the web decreases by increasing the values of velocities ratio.

¹School of Mathematics & Statistics, Xi'an Jiaotong University, Xi'an, Shaanxi, China

²Department of Mathematics, COMSATS University Islamabad, Abbottabad Campus, Abbottabad, Pakistan

³Department of Mathematics & Statistics, Riphah International University, Islamabad, Pakistan

Corresponding author:

Yanren Hou, School of Mathematics & Statistics, Xi'an Jiaotong University, Xi'an, Shaanxi 710049, China.

Email: yrhou@mail.xjtu.edu.cn

Keywords

Jeffrey fluids, magnetohydrodynamic, lubrication approximation theory, coating, reverse roll coating, heat transfer, numerical methods

Introduction

Coating phenomenon has developed a solid reputation due to its extensive application in industry. In numerous industrial procedures, thin liquid uniform coatings are formed on surfaces. Such procedures include photographic films, wrapping, coated items, magnetic records and beautification and protection of fabrics or metals with the coatings. These activities based on an extensive range of equipment. Roll coaters are commonly in use among these activities.^{1,2}

In the roll coating process, the space between the two rotating rolls is much smaller than their radii. This process is commonly categorized into groups such as: metering, forward and reverse rolls coating (RRC).³ The two rolls at the small gap (nip) co rotate in reverse and metering roll coating. For forward roll coating the rolls counter rotate. The coating material (liquid) forms a bath on the upstream side of the small gap and after exit from the nip, splits into two films of liquids, which are covered by the two surfaces of the rollers, one of which is added to the substrate for industrial purposes.⁴⁻⁶

In recent decades, the flow problems of roll coating techniques, including experimental work, theoretical and numerical analysis have been studied in detail. The forward roll coating was of vital significance amongst these and was the commonly discussed. Experimental investigation has been conducted on this by many scientists, whereas the theoretical research have been offered by Benkreira et al.,⁷ Greener and Middleman et al.,⁸ Zafar et al.,⁹ Zahid et al..¹⁰ Reverse roll coating has been much less considered compared to the forward roll coating analysis.¹¹

For the investigation of reverse roll coating systems, the earlier study by Greener et al.¹² and Holland et al.¹³ used the lubrication approximation theory to make simple the equations of motion, however, the study of the involvement of free surface, the influence of surface tension and fluid contact lines was not taken into consideration. Coyle et al.¹⁴ established a finite element method supported by experimental results to validate the significant fluid dynamics properties for reverse roll coating. They also demonstrated the presence of instabilities in flow, containing cascading and ribbing. Hao and Haber¹⁵ addressed the coating flow between two reverse rotating rolls by using the Galeriken finite element technique. Taylor and Zettlemoyer¹⁶ studied how ink flows in printing presses by using the principle of lubrication approximation. They achieved the effects of force and pressure distribution. Hintermaier and White¹⁷ addressed water flow between two rolls. They used the lubrication approximation theory and presented outcomes that were compatible with their experimental findings. A flawless reverse roll coating model was

developed by Belblidia et al.² using the Taylor-Galerkin pressure correction algorithm at highest velocity. The novelty of the work is motivated by the need in the coating manufacturing to coat stable, faster, and with uniform thin layers by optimizing the coater operating conditions and coating rheology. The theoretical research on coating during reverse roll of an incompressible, magnetohydrodynamic, non-isothermal, Casson fluid has been discussed by Ali et al.¹⁸ By utilizing the lubrication approximation principle, the governing flow equation added to the web in the simplified form was achieved. Analytical expressions for velocity profile, flow rate and pressure gradient have been demonstrated. Williamson fluid was studied by Ali et al.¹⁹ and some engineering parameters, such as coating thickness, power input, separation points, pressure distribution and roll separation force were discussed.

Many researchers have studied non-Newtonian fluid flow due to its several uses in industrial, engineering and scientific procedures, such as thermal and geothermal insulation, crude oil extraction and aerodynamics. The thermophysical properties of non-Newtonian fluids are important in these applications. In particular, their heat transfer property plays a key role in food processing, petroleum product manufacturing, polymer industries etc. The physical properties of such fluids cannot be described by a single Navier-Stoke equation.²⁰⁻²³ Different models have been established in the past according to certain material characteristics, like Maxwell and Oldroyd-B, second-fluid, Casson fluid, third-grade, Jeffrey fluid. The model under consideration is the Jeffrey fluid model. The Jeffrey fluid model describes the simple (linear) viscoelastic properties of fluids, which has extensive uses in the polymer industries. In the above listed applications, numerous scientists discussed Jeffrey fluid flow situations in various geometries. For illustration, Nadeem and Akram²⁴ considered the Jeffrey fluid for peristaltic flow in a rectangular duct. Srinivas and Muthuraj²⁵ concentrated their consideration in an inclined asymmetric channel to discuss the peristaltic flow of a Jeffrey fluid. Hayat et al.²⁶ used the homotopy analysis methodology to considered the generalized three-dimensional channel flow of a Jeffrey fluid. For medical and engineering processes, the fluid magnetic properties in fluid flows are important.

In several geophysical, astrophysical and engineering applications, MHD flows of electrically conductive fluid are discussed. The MHD principles are used by engineers to design heat exchangers, control and re-entry of vehicles, thermal safety, space propulsion, pumps and to develop novel power-generating systems. Another significant MHD feature is purifying molten metals by applying a magnetic field from non-metallic inclusions. All these MHD uses give lead to studying problems which involve the magnetohydrodynamic properties. For instance, Turkiymazoglu²⁷ explored both numerical and analytical solutions of MHD boundary layer flow of viscous fluid through a rotating sphere near the heat transfer equator. Bhattacharyya and Pop²⁸ studied the MHD boundary layer flow of viscous fluid caused by an exponentially shrinking sheet. Makinde²⁹ studied MHD

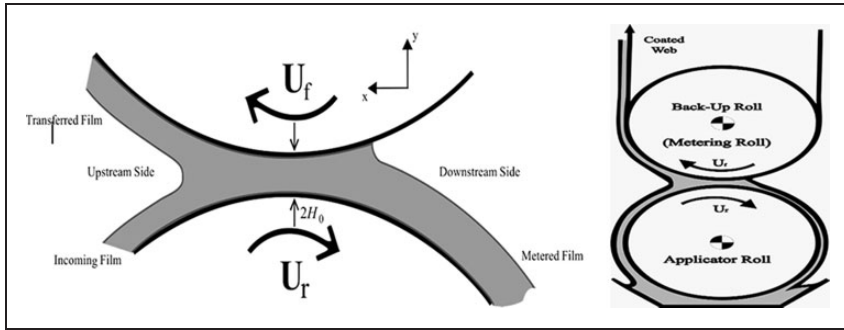


Figure 1. Reverse roll coating geometry.

viscous boundary layer fluid flow with Newtonian heating and Navier slip over a flat surface.

To the best of our knowledge, no literature is presented for the mathematical investigation of the reverse roll coating for MHD non-isothermal Jeffrey fluid. Thus, the purpose of the current study is to give the theoretical assessment of the Jeffrey fluid as it goes among two heated co-rotating rolls.

Mathematical formulation

Let us assume steady, non-isothermal and MHD flow of an incompressible Jeffrey fluid. The two identical radii R rolls lie in the plane of free surface and parallel to each other that co-rotate with Peripheral velocities (U_r and U_f), where the subscripts r stands for reverse and f stands for forward rotating rolls. The narrow gap called nip region is maintained between the co-rotating rolls and is denoted by $2H_0$. The coating flow is dragged through the reverse roll (applicator roll) into the nip region between the two rolls. Furthermore, the x – axis and y – axis are in the flow direction and transverse to the flow (see Figure 1).

The basic equations that govern the MHD flow of a steady, non-isothermal fluid are

$$\text{div } \bar{\mathbf{U}} = 0 \quad (1)$$

$$\rho \frac{D\bar{\mathbf{U}}}{Dt} = \text{div} \mathbf{T} - \nabla p + \mathbf{J} \times \mathbf{B} \quad (2)$$

$$\rho C_p \frac{D\theta}{Dt} = k \nabla^2 \theta + \mathbf{T} \cdot \nabla \bar{\mathbf{U}} \quad (3)$$

where

ρ	=	fluid density
C_p	=	specific heat capacity
θ	=	Temperature
$\nabla \bar{\mathbf{U}}$	=	velocity gradient
t	=	Time
k	=	thermal conductivity
$\frac{D}{Dt}$	=	material time derivative
$\bar{\mathbf{U}}$	=	fluid velocity
\mathbf{J}	=	current density
\mathbf{B}	=	total magnetic field.
\mathbf{T}	=	Jeffrey fluid model ³⁰ extra stress tensor That satisfies the constitutive equation below

$$\mathbf{T} = \frac{\mu}{1 + \lambda_1} \left(\mathbf{A}_1 + \lambda_2 \frac{D\mathbf{A}_1}{Dt} \right) \tag{4}$$

$$\frac{D(\cdot)}{Dt} = \frac{\partial(\cdot)}{\partial t} + (\bar{\mathbf{U}} \cdot \nabla)(\cdot) \tag{5}$$

$$\mathbf{A}_1 = (\nabla \bar{\mathbf{U}}) + (\nabla \bar{\mathbf{U}})^T \tag{6}$$

where

λ_1	=	Jeffrey fluid parameter (relaxation time divided by retardation time)
μ	=	fluid dynamic viscosity
λ_2	=	retardation time.

The velocity profile for fluid flow is

$$\bar{\mathbf{U}} = [u(x, y), v(x, y)], \quad T = T(x, y) \tag{7}$$

In above equation (7), u and v represents the velocity components in x -direction and y -direction and

$$\mathbf{A}_1 = \begin{pmatrix} 2\frac{\partial u}{\partial x} & \frac{\partial v}{\partial x} + \frac{\partial u}{\partial y} \\ \frac{\partial v}{\partial x} + \frac{\partial u}{\partial y} & 2\frac{\partial v}{\partial y} \end{pmatrix}$$

We assume that the electric field is zero and related with the applied magnetic field, the induced magnetic field is weak enough that the magnetic Reynolds number is minimal and negligible.³¹ Then the Lorentz force $\mathbf{J} \times \mathbf{B}$ becomes $\sigma(\bar{\mathbf{U}} \times \mathbf{B}) \times \mathbf{B}$ (where σ denotes the fluid electric conductivity). Therefore, the applied magnetic field B_0 only adds to the electrical density. In this case, because of magnetic field the Lorentz force becomes

$$\mathbf{J} \times \mathbf{B} = -\sigma B_0^2 \bar{\mathbf{U}} \quad (8)$$

In view of equations (1), (4) and (5), equations (2) and (3) can be written as

$$\rho \left(u \frac{\partial u}{\partial x} + v \frac{\partial u}{\partial y} \right) = \frac{\partial \tau_{xx}}{\partial x} + \frac{\partial \tau_{xy}}{\partial y} - \frac{\partial p}{\partial x} - \sigma B_0^2 u \quad (9)$$

$$\rho \left(u \frac{\partial v}{\partial x} + v \frac{\partial v}{\partial y} \right) = \frac{\partial \tau_{yx}}{\partial x} + \frac{\partial \tau_{yy}}{\partial y} - \frac{\partial p}{\partial y} - \sigma B_0^2 v \quad (10)$$

$$\rho C_p \left(u \frac{\partial \theta}{\partial x} + v \frac{\partial \theta}{\partial y} \right) = k \left(\frac{\partial^2 \theta}{\partial x^2} + \frac{\partial^2 \theta}{\partial y^2} \right) + \tau_{xx} \frac{\partial u}{\partial x} + \tau_{xy} \left(\frac{\partial u}{\partial y} + \frac{\partial v}{\partial x} \right) + \tau_{yy} \frac{\partial v}{\partial y} \quad (11)$$

where τ_{yy} , τ_{xx} , τ_{xy} and τ_{yx} are the stress components.

We start with the LAT that in the nip region of the reverse-roll coating process, where the most significant dynamic events happen. The roll surfaces are almost parallel in that area, and move to either side for a small distance. Then it is reasonable to assume that $u \gg v$ and $\frac{\partial}{\partial y} \gg \frac{\partial}{\partial x}$. The fluid travels in the x -direction and there is no velocity in the y -direction. This discussion leads the above equations into the following simplified form

$$\frac{\mu}{1 + \lambda_1} \frac{d^2 u}{dy^2} - \sigma B_0^2 u = \frac{dp}{dx} \quad (12)$$

$$\frac{dp}{dy} = 0 \quad (13)$$

$$k \frac{d^2 \theta}{dy^2} + \frac{\mu}{1 + \lambda_1} \left(\frac{du}{dy} \right)^2 = 0 \quad (14)$$

From equation (13), it is clear that p is not a function of y , i.e., $p \neq p(y)$. This means p is a function of x , i.e., $p = p(x)$.

A suitable boundary condition is

$$\left. \begin{aligned} u &= -U_r \text{ at } y = \sigma \\ u &= U_f \text{ at } y = -\sigma \end{aligned} \right\} \quad (15)$$

Dimensionless equation

In this section, the governing equations of Jeffrey fluid for reverse roll coating process in dimensionless form are presented. Suppose the following suitable dimensionless variables ¹²

$$\left. \begin{aligned} x^* &= \frac{x}{\sqrt{RH_0}}, \quad u^* = \frac{u}{U_f}, \quad y^* = \frac{y}{H_0}, \quad p^* = \sqrt{\frac{H_0}{R}} \frac{pH_0}{\mu U_f}, \quad \theta^* = \frac{\theta - \theta_0}{\theta_1 - \theta_0} \\ \tau_{xy} &= \frac{\tau_{xy} H_0}{\mu U_f}, \quad \tau_{xx} = \frac{\tau_{xx} H_0}{\mu U_f}, \quad \tau_{yy} = \frac{\tau_{yy} H_0}{\mu U_f} \end{aligned} \right\} \quad (16)$$

In view of above dimensionless variables, equations (12) and (14) can be written as after removing ‘*’ for convenience

$$N \frac{d^2 u}{dy^2} - M^2 u = \frac{dp}{dx} \quad (17)$$

$$\frac{d^2 \theta}{dy^2} + BrN \left(\frac{du}{dy} \right)^2 = 0 \quad (18)$$

where

M	$=$	$\sqrt{\frac{\sigma}{\mu}} H_0 B_0$
N	$=$	$\frac{1}{1 + \lambda_1}$
Br	$=$	$\frac{\mu C_p}{k} \times \frac{U_f^2}{C_p(\theta_1 - \theta_0)} = Ec \times Pr$
Pr	$=$	Prandtl number
Ec	$=$	Eckert number

Pr = the Prandtl

Ec = Eckert number

Their product represents the Brickman number Br which represents the viscous heating relative to the conductive heat transfer.

Appropriate kinematic dimensionless boundary condition¹² are

$$\left. \begin{aligned} u &= 1 \quad \text{at} \quad y = -\sigma \\ u &= -k \quad \text{at} \quad y = \sigma \\ \theta &= 0 \quad \text{at} \quad y = -\sigma \\ \theta &= 1 \quad \text{at} \quad y = \sigma \end{aligned} \right\} \quad (19)$$

where $k = \frac{U_r}{U_f}$ and the boundary roll surface are denoted as $y = \pm\sigma(x) = 1 + \frac{x^2}{2}$.

Mathematical results

The solution of equation (17) by utilizing the boundary conditions defined in equation (19) becomes

$$u = -\frac{\left(kM^2 - M^2 - 2\frac{dp}{dx}\right)\cosh\left(\frac{My}{\sqrt{N}}\right) - (k+1)\sinh\left(\frac{My}{\sqrt{N}}\right)}{2M^2\cosh\left(\frac{M\sigma}{\sqrt{N}}\right)} - \frac{1}{M^2}\frac{dp}{dx} \quad (20)$$

The dimensionless flow rate through the nip is

$$\lambda = \frac{1}{2} \int_{-\sigma}^{\sigma} u(y) dy \quad (21)$$

or

$$\lambda = \frac{1}{8M^3\sinh\left(\frac{M\sigma}{\sqrt{N}}\right)\cosh\left(\frac{M\sigma}{\sqrt{N}}\right)} \left[e^{\frac{-2M\sigma}{\sqrt{N}}} \left(\begin{aligned} &\left(\sqrt{N}M^2(1-k) + 2(\sqrt{N} - \sigma M)\frac{dp}{dx} \right) e^{\frac{4M\sigma}{\sqrt{N}}} \\ &- 2\left(2\sqrt{N}\frac{dp}{dx} + M^2\sqrt{N}(1-k) \right) e^{\frac{2M\sigma}{\sqrt{N}}} \\ &- M^2\sqrt{N}(k-1) + 2(M\sigma + \sqrt{N})\frac{dp}{dx} \end{aligned} \right) \right] \quad (22)$$

From equation (20) and equation (21), we have

$$\frac{dp}{dx} = T \left(\begin{array}{l} 8 M \cosh\left(\frac{M\sigma}{\sqrt{N}}\right) \sinh\left(\frac{M\sigma}{\sqrt{N}}\right) \lambda - 2 \sqrt{N} k \\ + \sqrt{N} e^{2\frac{M\sigma}{\sqrt{N}}} k + 2 \sqrt{N} - \sqrt{N} e^{2\frac{M\sigma}{\sqrt{N}}} \\ + \sqrt{N} e^{-2\frac{M\sigma}{\sqrt{N}}} k - \sqrt{N} e^{-2\frac{M\sigma}{\sqrt{N}}} \end{array} \right) \quad (23)$$

where

$$T = - \frac{M^2}{e^{-2\frac{M\sigma}{\sqrt{N}}} \left(M e^{\frac{4M\sigma}{\sqrt{N}}} \sigma - M\sigma + 2 \sqrt{N} e^{\frac{2M\sigma}{\sqrt{N}}} - \sqrt{N} e^{\frac{4M\sigma}{\sqrt{N}}} - \sqrt{N} \right)}$$

The exact solution of equation (23) is hard to find. So, the numerical method called trapezoidal rule with a predefined accuracy of 10^{-10} is used with boundary condition $p = 0$ as $x \rightarrow -\infty$ to obtain numerical results for the pressure.

A second simple material balance relationship for λ is defined as

$$U_f H_f - U_r H_r = 2\lambda H_0 U_f \quad (24)$$

where U_r and U_f are the reverse and forward roll velocities.

Equation (24) leads to expression which is given by

$$v = \frac{H_f}{H_r} = k + 2\beta\lambda \quad (25)$$

where $v = \frac{H_f}{H_r}$ is the coating thickness, $\beta = \frac{H_0}{H_r}$, where H_0 is half the nip separation gap between two rolls and H_f , H_r denote the forward fluid film thickness and the reverse fluid film thickness. So, we need the flow rate $\lambda(k)$ to calculate the coating thickness and pressure distribution.

To determine $\lambda(k)$, impose Swift Stieber-boundary conditions on pressure distributions. It is asserted that at the separation point $x = x_{sp}$ where the lubrication type flow transforms into a transverse flow, both the pressure and pressure gradient vanished. On setting $\frac{dp}{dx} = 0$ in equation (23) we get

$$\sigma_t = 1 + \frac{1}{2} x_{sp}^2 = \frac{\sqrt{N}}{M} \tanh^{-1} \left(\frac{2\lambda M}{(1-k)\sqrt{N}} \right) \quad (26)$$

In view of the Swift-Stieber boundary condition on pressure, replacing x with x_{sp} everywhere in the obtained result for pressure distribution from equation (23),

finding x_{sp} in terms of λ from the equation (26), and substituting into resulting equation of pressure distribution, transcendental equation in λ is obtained and then numerical method named as Newton-Raphson method is used to get λ , which Tables 1 to 3 show.

Table 1. Effect of k on flow rate λ , separation points x_{sp} , coating thickness ν , power input p_w and force F .

k	λ	x_{sp}	ν	p_w	F
0.1	0.6745	1.00023	1.3141	-0.55532	-0.11816
0.2	0.5994	0.99984	1.2789	-0.55763	-0.10477
0.3	0.5244	0.99963	1.2439	-0.56035	-0.09168
0.4	0.4494	0.99934	1.2089	-0.56305	-0.07858
0.5	0.3744	0.99894	1.1739	-0.56572	-0.06530
0.6	0.2994	0.99834	1.1389	-0.56835	-0.05213
0.7	0.2245	0.99801	1.1041	-0.57116	-0.03894
0.8	0.1496	0.99733	1.0692	-0.57389	-0.02595
0.9	0.0747	0.88532	1.0344	-0.57632	-0.01287

Table 2. Effect of M on flow rate λ , separation points x_{sp} , coating thickness ν , power input p_w and force F .

M	λ	x_{sp}	ν	p_w	F
0.1	0.6602	0.99997	1.2883	-0.53823	-0.11404
0.2	0.6201	0.99981	1.2161	-0.49161	-0.10276
0.3	0.5649	0.99971	1.1168	-0.42885	-0.08751
0.4	0.5050	0.99968	1.0090	-0.36315	-0.07133
0.5	0.4475	0.99883	0.9055	-0.30318	-0.05621
0.6	0.3962	0.99852	0.8131	-0.25344	-0.04339
0.7	0.3520	0.99744	0.7336	-0.21441	-0.03293
0.8	0.3141	0.97674	0.6653	-0.18363	-0.02356
0.9	0.2829	0.97344	0.6092	-0.16298	-0.01753

Table 3. Effect of λ_1 on flow rate λ , separation points x_{sp} , coating thickness v , power input p_w and force F .

λ_1	λ	x_{sp}	v	p_w	F
1	0.67459	0.99998	1.3142	−0.83269	−0.17703
2	0.67437	0.99994	1.3138	−0.55486	−0.11791
3	0.67416	0.99993	1.3134	−0.41595	−0.08843
4	0.67395	0.99991	1.3131	−0.33261	−0.07071
5	0.67374	0.99989	1.3127	−0.27705	−0.05891
6	0.67353	0.99987	1.3123	−0.23736	−0.05048
7	0.67332	0.99985	1.3119	−0.20760	−0.04413
8	0.67311	0.99983	1.3115	−0.18445	−0.03919
9	0.67928	0.99981	1.3113	−0.16596	−0.03527

Temperature distribution

Upon using equation (20) into the non-dimensional form of energy equation (18), we get

$$\frac{d^2\theta}{dy^2} + BrN \left[-\frac{\left(kM^2 - M^2 - 2\frac{dp}{dx}\right)\sinh\left(\frac{My}{\sqrt{N}}\right)}{2M\sqrt{N}\cosh\left(\frac{M\sigma}{\sqrt{N}}\right)} - \frac{(k+1)M\cosh\left(\frac{My}{\sqrt{N}}\right)}{2\sqrt{N}\sinh\left(\frac{M\sigma}{\sqrt{N}}\right)} \right]^2 = 0 \quad (27)$$

where $\frac{dp}{dx}$ is defined in equation (23). Solving equation (27) subject to boundary conditions in equation (19), we get

$$\theta = \frac{1}{32\sigma M^4 \cosh\left(\frac{M\sigma}{\sqrt{N}}\right)^2 \sinh\left(\frac{M\sigma}{\sqrt{N}}\right)^2} \times \left[A \left(\cosh\left(\frac{2M\sigma}{\sqrt{N}}\right) - \cosh\left(\frac{2My}{\sqrt{N}}\right) \right) - 2M^2 B \left(\sigma \sinh\left(\frac{2My}{\sqrt{N}}\right) - y \sinh\left(\frac{2M\sigma}{\sqrt{N}}\right) \right) + \right. \\ \left. (y + \sigma) \left(-8M^2 \cosh\left(\frac{M\sigma}{\sqrt{N}}\right)^4 + \left(8 + 4\frac{dp}{dx}\sigma(y - \sigma)(k - 1)Br \right) M^2 - \cosh\left(\frac{M\sigma}{\sqrt{N}}\right)^2 \right. \right. \\ \left. \left. + Br\sigma(y - \sigma) \left(4\left(\frac{dp}{dx}\right)^2 Br\sigma(y - \sigma) + Br\sigma(y - \sigma) \left((k - 1)M^2 - 2\frac{dp}{dx} \right)^2 \right) \right) \cosh\left(\frac{M\sigma}{\sqrt{N}}\right)^2 \right] \quad (28)$$

where

$$A = 2 \left(\left((k^2 + 1)M^2 - 2M^2 \frac{dp}{dx} (k - 1) + 2 \left(\frac{dp}{dx} \right)^2 \right) \cosh \left(\frac{M\sigma}{\sqrt{N}} \right)^2 - \frac{\left((k - 1)M^2 - 2 \frac{dp}{dx} \right)^2}{2} \right) Br\sigma N$$

and

$$B = BrNs \sinh \left(\frac{M\sigma}{\sqrt{N}} \right) \cosh \left(\frac{M\sigma}{\sqrt{N}} \right) \left(M^2(k - 1) - 2 \frac{dp}{dx} \right) (1 + k).$$

Operating variables

Once the pressure gradients, velocity profile and pressure distributions are achieved, operating variables such as power input and separation force etc. are easily found.

Separating force

The dimensionless roll separating $F^{22,32}$ force is

$$F = \frac{\bar{F}H_0}{\mu URW} = \int_{-\infty}^{x_t} p(x) dx \quad (29)$$

where \bar{F} and F denote the dimensional and dimensionless roll separating force per unit width W .

Power input

The power transferred^{22,32} to the fluid by the roll is obtained by the integral

$$P_w = \frac{\bar{P}}{\mu W U^2} = \int_{-\infty}^{x_t} \tau_{xy}(x, 1) dx \quad (30)$$

Here P_w denotes the non-dimension power and non-dimension form of share stress component is

$$\tau_{xy} = \frac{1}{1 + \lambda_1} \frac{\partial u}{\partial y} \quad (31)$$

Nusselt number

The Nu (Nusselt number) at upper roll surface is defined as

$$Nu = \left| \frac{d\theta}{dy} \right|_{\sigma} \quad (32)$$

On differentiating equation (29) and using into equation (32), we get

$$Nu = \frac{1}{32 \left(e^{\frac{M\sigma}{\sqrt{N}}} \right)^2 M^3 \sigma \sinh \left(\frac{M\sigma}{\sqrt{N}} \right)^2 \cosh \left(\frac{M\sigma}{\sqrt{N}} \right)^2} \times \left[\begin{aligned} & 16M^3 \cosh \left(\frac{M\sigma}{\sqrt{N}} \right)^4 \left(e^{\frac{M\sigma}{\sqrt{N}}} \right)^2 \\ & + \left(-2\sigma\sqrt{N} \left(M^4(1+k^2) - 2\frac{dp}{dx}(k-1)M^2 + 2\left(\frac{dp}{dx}\right)^2 \right) Br \left(\frac{M\sigma}{\sqrt{N}} \right)^4 \right. \\ & + \left. -16 \left(\sigma^2 \left(M^2 + \frac{dp}{dx} \right) \left(M^2k - \frac{dp}{dx} \right) Br + M^2 \right) M \left(\frac{M\sigma}{\sqrt{N}} \right)^2 \right. \\ & + \left. +2\sigma\sqrt{N} \left(M^4(1+k^2) - 2\frac{dp}{dx}(k-1)M^2 + 2\left(\frac{dp}{dx}\right)^2 \right) Br \right) \cosh \left(\frac{M\sigma}{\sqrt{N}} \right)^2 \\ & - 2M \sinh \left(\frac{M\sigma}{\sqrt{N}} \right) \left(\left(M\sigma\sqrt{N} - \frac{N}{2} \right) \left(e^{\frac{M\sigma}{\sqrt{N}}} \right)^4 + M\sigma\sqrt{N} + \frac{N}{2} \right) \\ & \times \left(-2\frac{dp}{dx} + M^2(k-1) \right) Br(k+1) \cosh \left(\frac{M\sigma}{\sqrt{N}} \right) \\ & - 4\sigma \left(-\frac{\sqrt{N} \left(e^{\frac{M\sigma}{\sqrt{N}}} \right)^4}{4} + M\sigma \left(e^{\frac{M\sigma}{\sqrt{N}}} \right)^2 + \frac{\sqrt{N}}{4} \right) \left(M^2(k-1) - 2\frac{dp}{dx} \right)^2 Br \end{aligned} \right] \quad (33)$$

Also

$$Nu = \left| \frac{d\theta}{dy} \right|_{-\sigma} \quad (34)$$

or

$$Nu = \frac{1}{32 \left(\frac{M\sigma}{\sqrt{N}}\right)^2 M^3 \sigma \sinh\left(\frac{M\sigma}{\sqrt{N}}\right)^2 \cosh\left(\frac{M\sigma}{\sqrt{N}}\right)^2}$$

$$\times \left[\begin{aligned} &16 M^3 \cosh\left(\frac{M\sigma}{\sqrt{N}}\right)^4 \left(\frac{M\sigma}{\sqrt{N}}\right)^2 \\ &+ \left(2\sigma\sqrt{N} \left((k^2 + 1)M^4 - 2\frac{dp}{dx}(k-1)M^2 + 2\left(\frac{dp}{dx}\right)^2 \right) Br \left(\frac{M\sigma}{\sqrt{N}}\right)^4 \right. \\ &+ 16 \left(\sigma^2 \left(M^2 + \frac{dp}{dx} \right) \left(M^2 k - \frac{dp}{dx} \right) Br - M^2 \right) M \left(\frac{M\sigma}{\sqrt{N}}\right)^2 \\ &\left. - 2\sigma\sqrt{N} \left(M^4(1+k^2) - 2\frac{dp}{dx}(k-1)M^2 + 2\left(\frac{dp}{dx}\right)^2 \right) Br \right) \cosh\left(\frac{M\sigma}{\sqrt{N}}\right)^2 \\ &- 2M \sinh\left(\frac{M\sigma}{\sqrt{N}}\right) \left(\left(M\sigma\sqrt{N} - \frac{N}{2} \right) \left(\frac{M\sigma}{\sqrt{N}}\right)^4 \right. \\ &\quad \left. + M\sigma\sqrt{N} + \frac{N}{2} \right) \\ &\times \left(M^2(k-1) - 2\frac{dp}{dx} \right) Br (1+k) \cosh\left(\frac{M\sigma}{\sqrt{N}}\right) + \\ &4\sigma \left(-\frac{\sqrt{N}\left(\frac{M\sigma}{\sqrt{N}}\right)^4}{4} + M\sigma \left(\frac{M\sigma}{\sqrt{N}}\right)^2 + \frac{\sqrt{N}}{4} \right) \left((k-1)M^2 - 2\frac{dp}{dx} \right)^2 Br \end{aligned} \right]$$

(35)

Table 4. Effect of nip gap $\beta = \frac{H_0}{H_r}$ on coating thickness.

$k = 0.1,$ $\lambda = 0.6745$ $\beta = \frac{H_0}{H_r}$	$v = \frac{H_r}{H_t}$	$M = 0.3,$ $\lambda = 0.5449$ $\beta = \frac{H_0}{H_r}$	$v = \frac{H_r}{H_t}$	$\lambda_1 = 8,$ $\lambda = 0.6731$ $\beta = \frac{H_0}{H_r}$	$v = \frac{H_r}{H_t}$
0.1	0.2349	0.1	0.2089	0.1	0.2346
0.2	0.3698	0.2	0.3179	0.2	0.3692
0.3	0.5047	0.3	0.4269	0.3	0.5038
0.4	0.6396	0.4	0.5359	0.4	0.6384
0.5	0.7745	0.5	0.6449	0.5	0.7731
0.6	0.9094	0.6	0.7538	0.6	0.9077
0.7	1.0443	0.7	0.8628	0.7	1.0423
0.8	1.1792	0.8	0.9718	0.8	1.1769
0.9	1.3141	0.9	1.0808	0.9	1.3115

Table 5. Effect of k on flow rate λ_0 , separation points x_0 , coating thickness v_0 (Newtonian case).

k	λ_0	x_0	v_0
0.1	0.5516	0.6719	1.0928
0.2	0.4903	0.6718	1.0825
0.3	0.4290	0.6717	1.0722
0.4	0.3677	0.6716	1.0618
0.5	0.3064	0.6715	1.0515
0.6	0.2451	0.6714	1.0411
0.7	0.1838	0.6713	1.0308
0.8	0.1226	0.6708	1.0206
0.9	0.0612	0.6693	1.0101

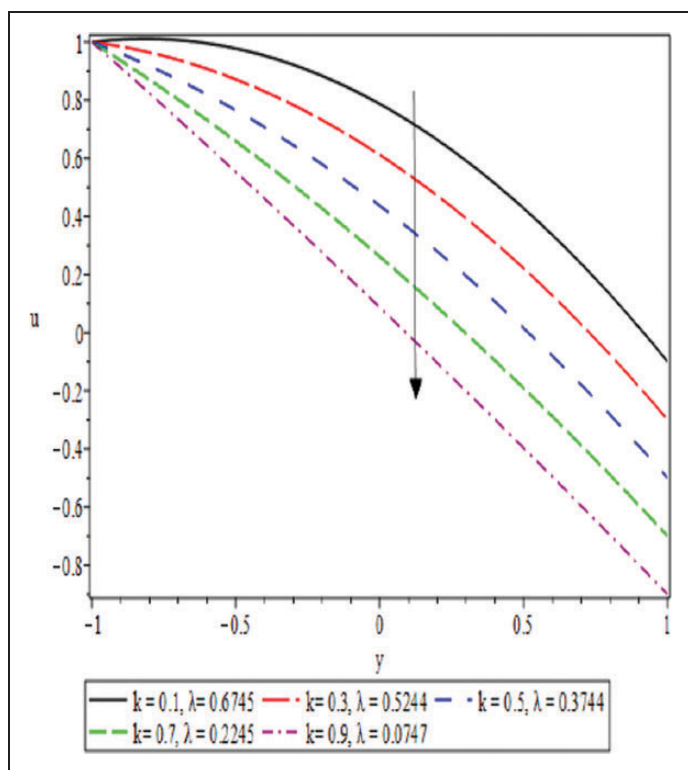


Figure 2. Impact of k on velocity distribution at $x = 0$.

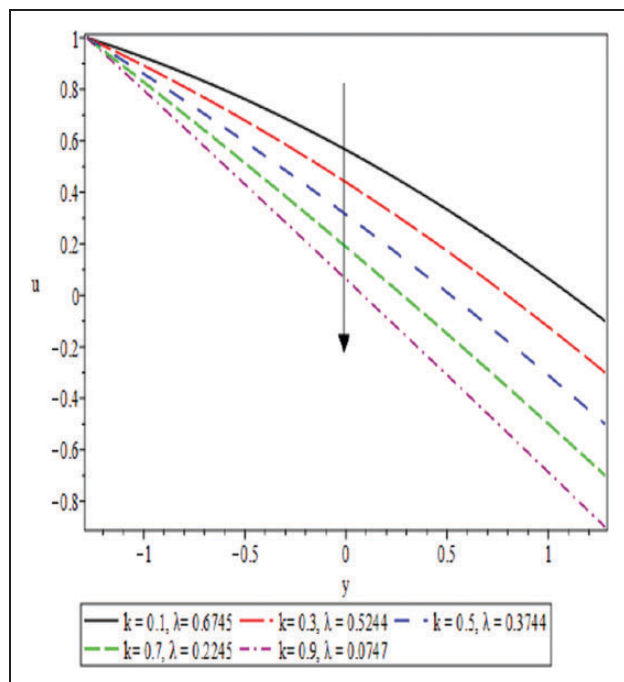


Figure 3. Impact of k on velocity distribution at $x = 0.75$.

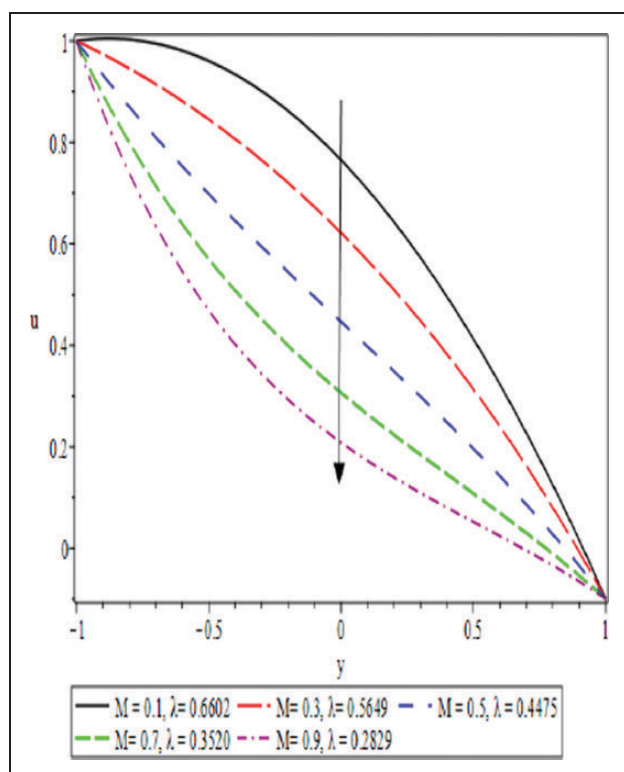


Figure 4. Impact of M on velocity distribution at $x = 0$.

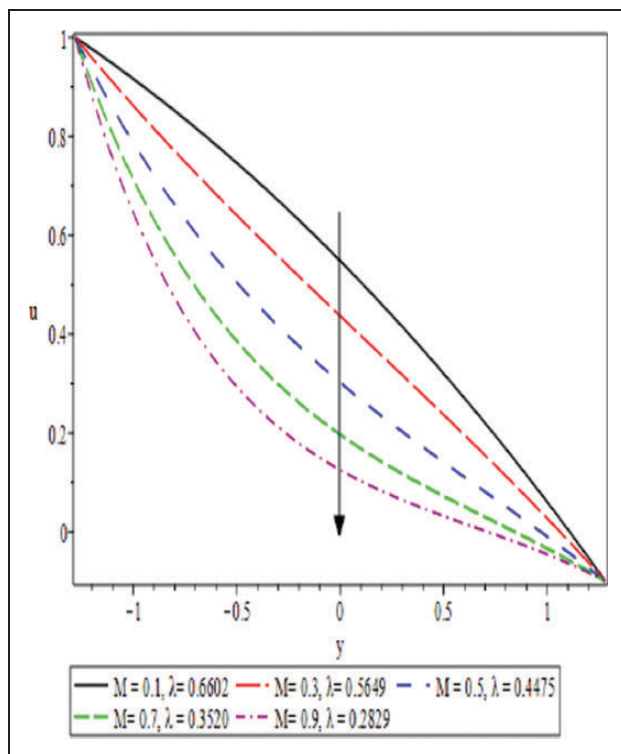


Figure 5. Impact of M on velocity distribution at $x = 0.75$.

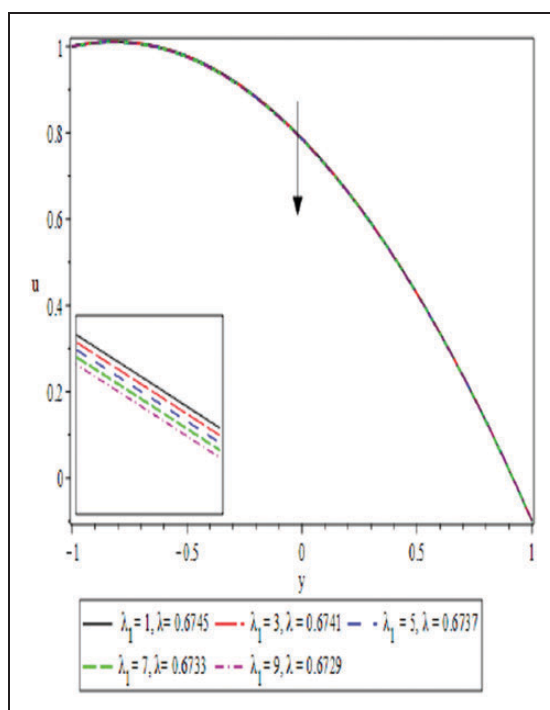


Figure 6. Impact of λ_1 on velocity distribution at $x = 0$.

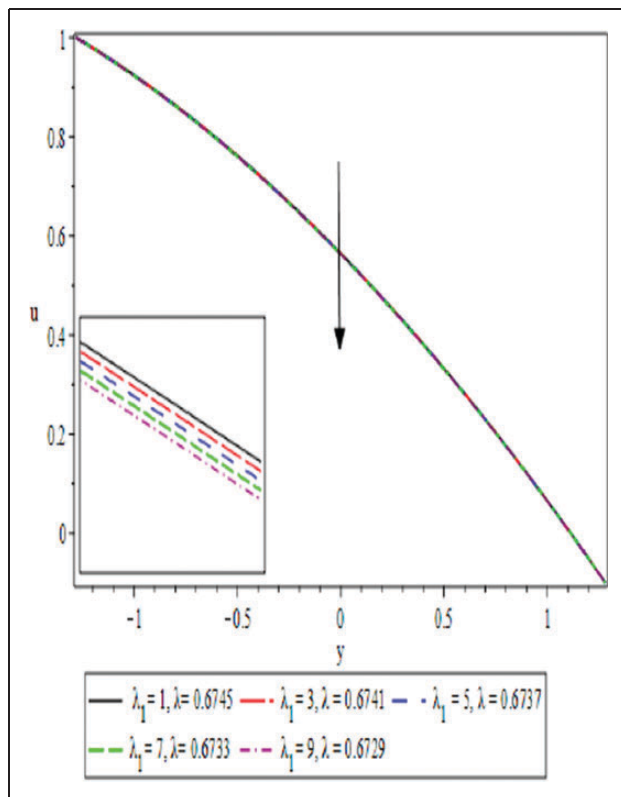


Figure 7. Impact of λ_1 on velocity distribution at $x = 0.75$.

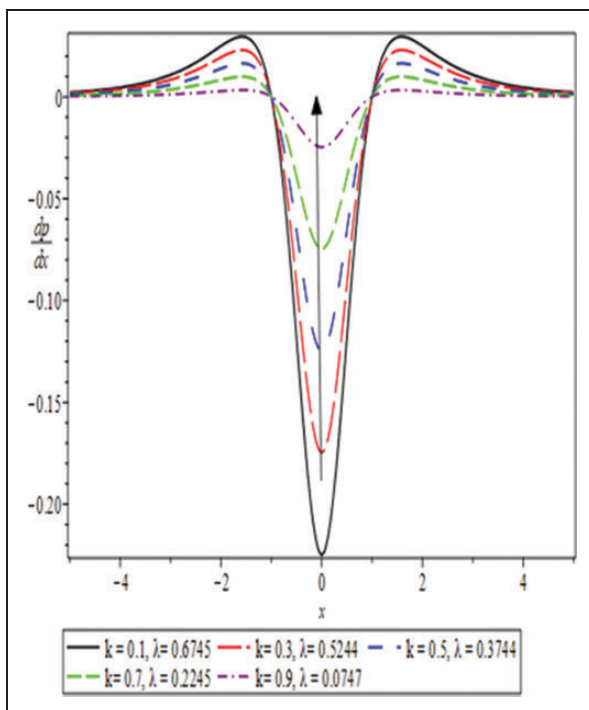


Figure 8. Impact of k on pressure gradient.

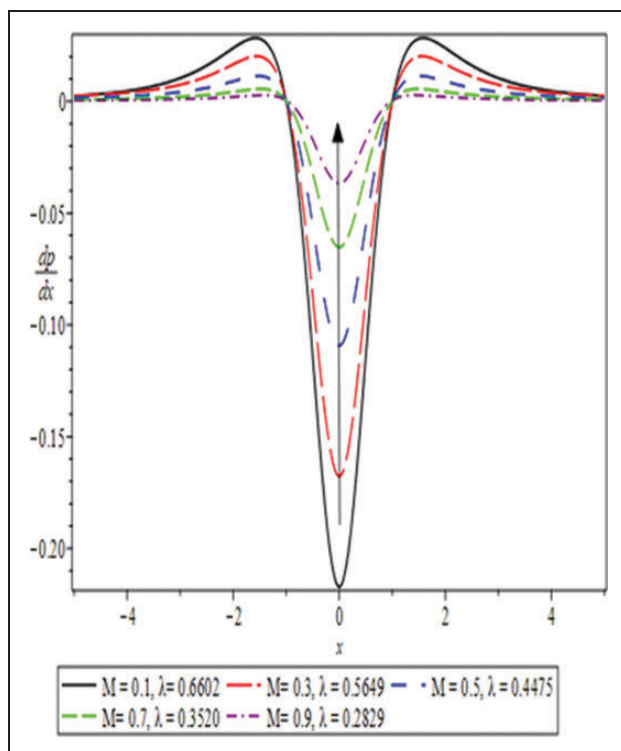


Figure 9. Impact of M on pressure gradient.

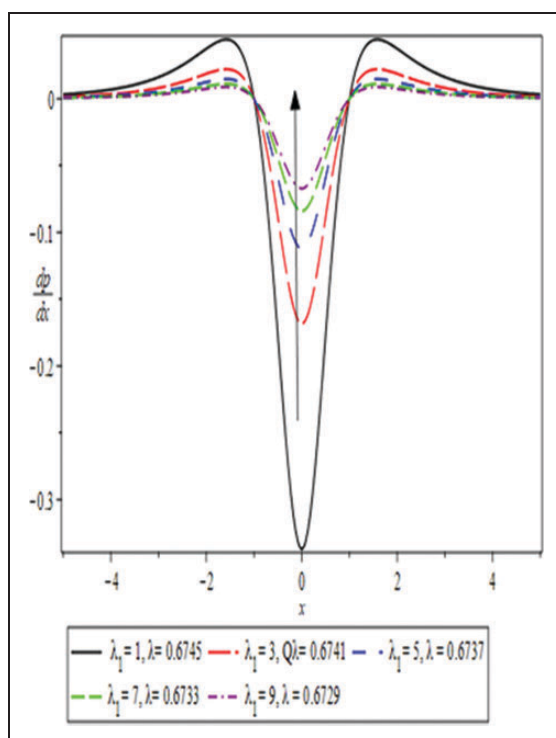


Figure 10. Impact of λ_1 on pressure gradient.

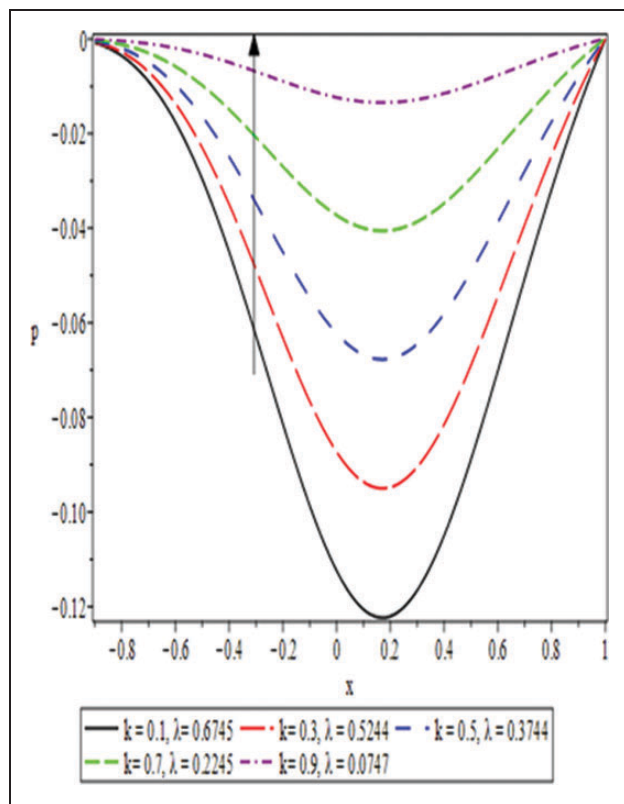


Figure 11. Impact of k on pressure distribution.

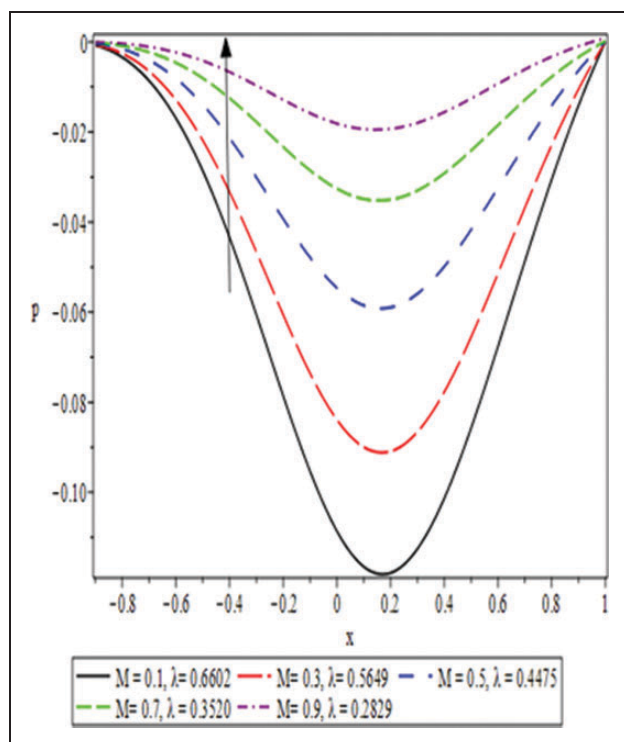


Figure 12. Impact of M on pressure distribution.

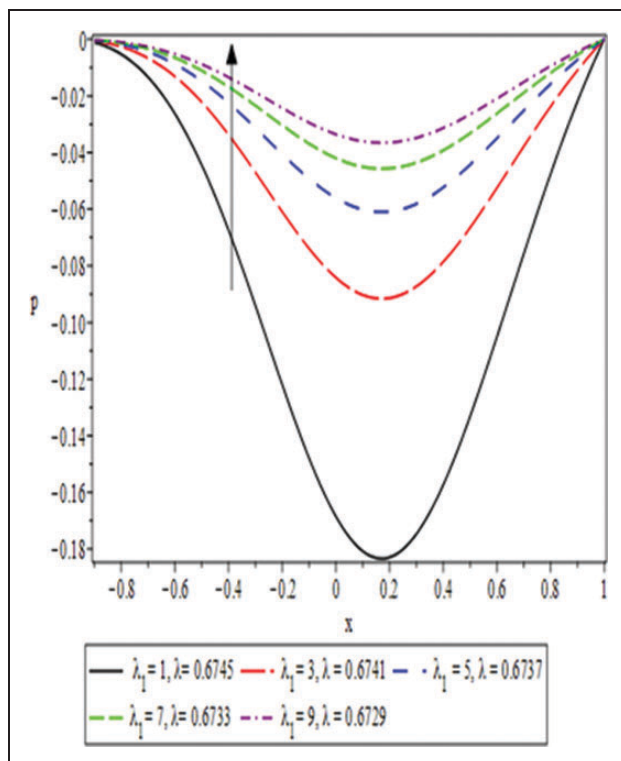


Figure 13. Impact of λ_1 on pressure distribution.

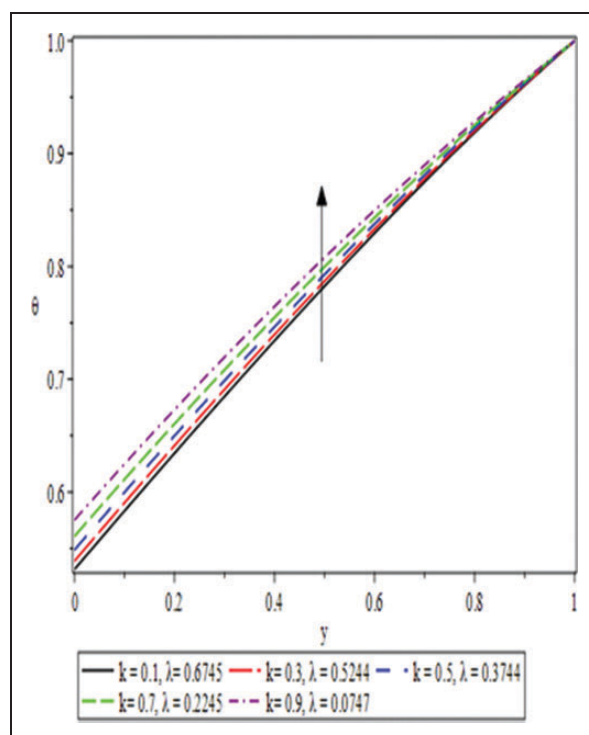


Figure 14. Impact of k on Temperature profile at $x = 0$.

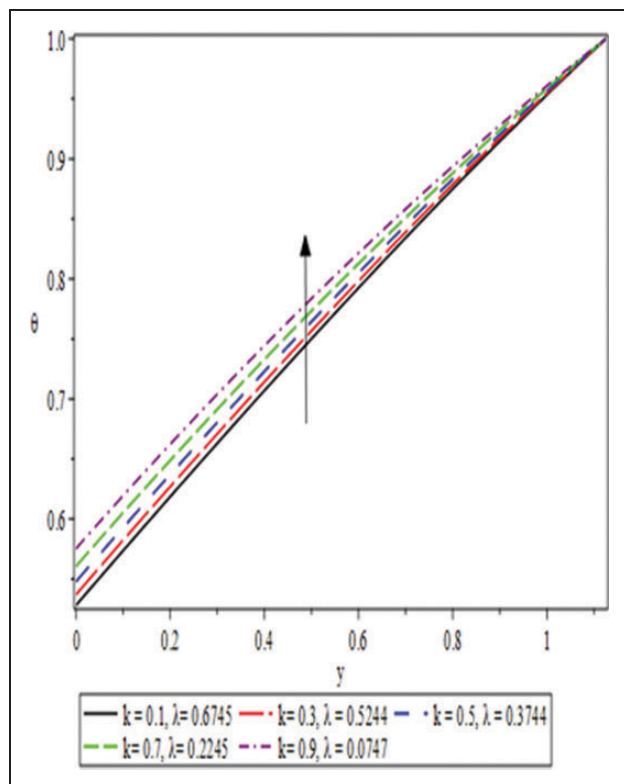


Figure 15. Impact of k on Temperature profile at $x = 0.5$.

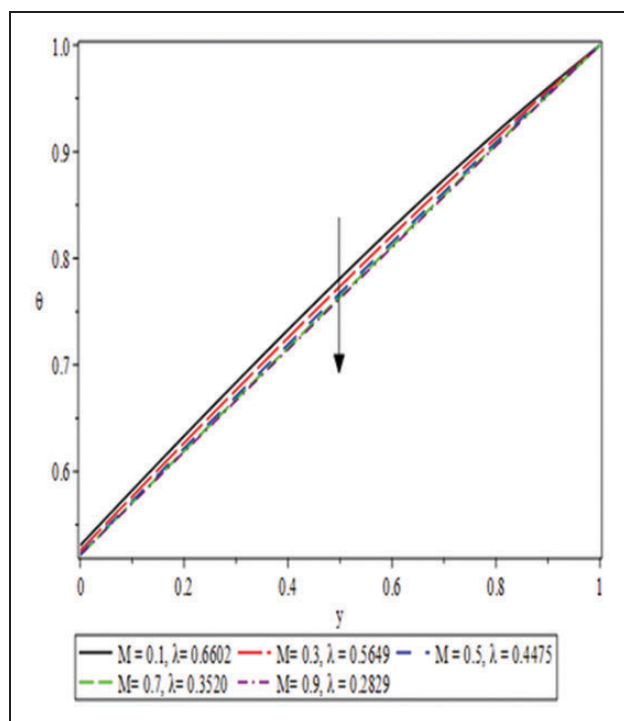


Figure 16. Impact of M on Temperature profile at $x = 0$.

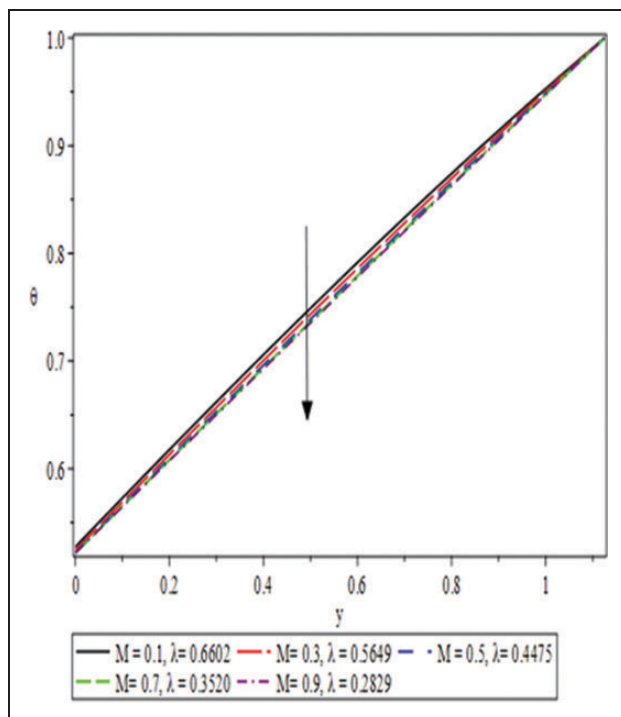


Figure 17. Impact of M on Temperature profile at $x = 0.5$.

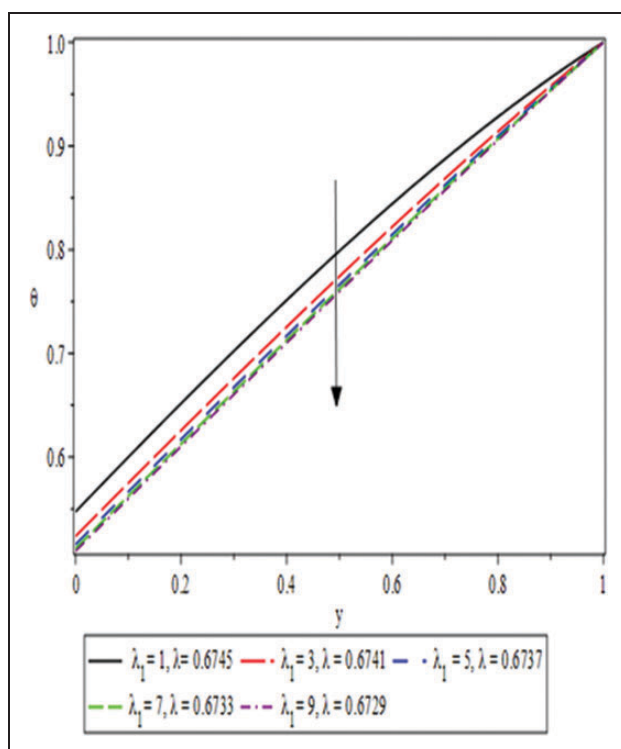


Figure 18. Impact of λ_1 on Temperature profile at $x = 0$.

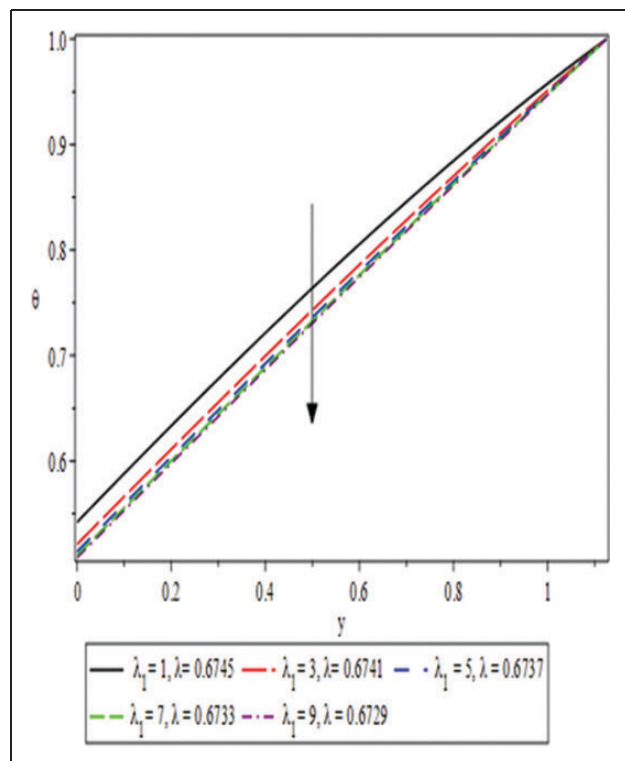


Figure 19. Impact of λ_1 on Temperature profile at $x = 0.5$.

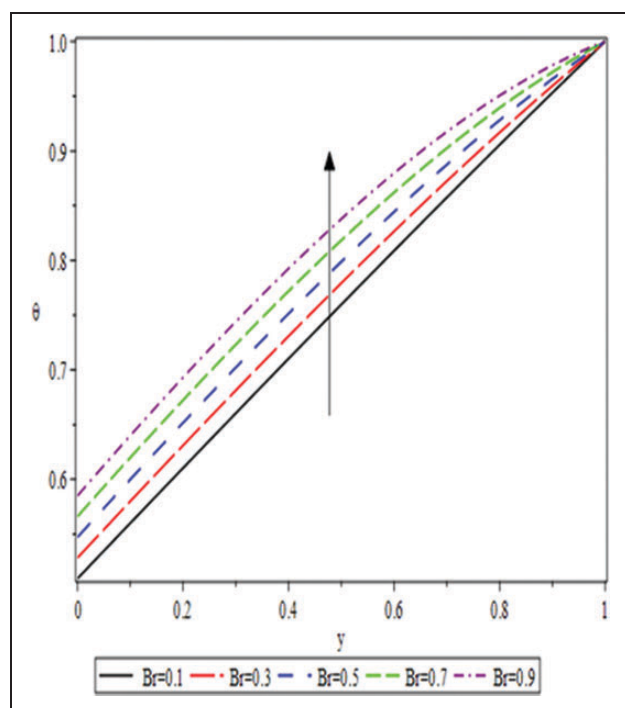


Figure 20. Impact of Br on Temperature profile at $x = 0$.

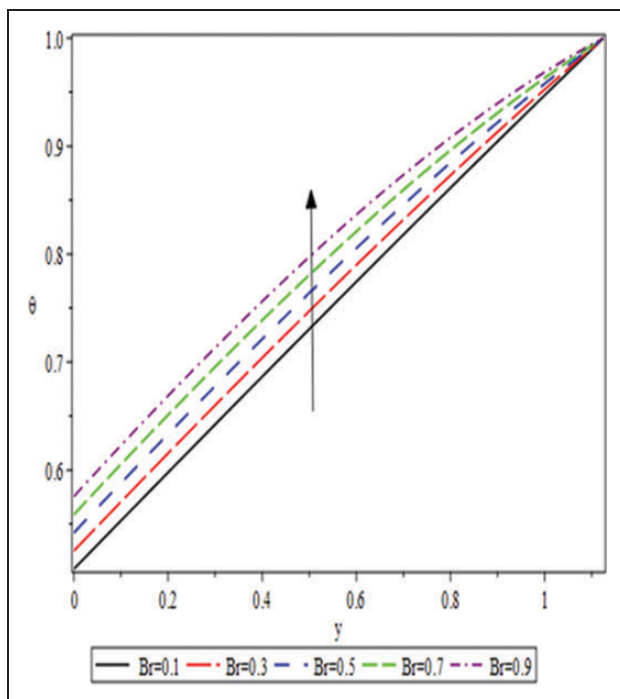


Figure 21. Impact of Br on Temperature profile at $x = 0.5$.

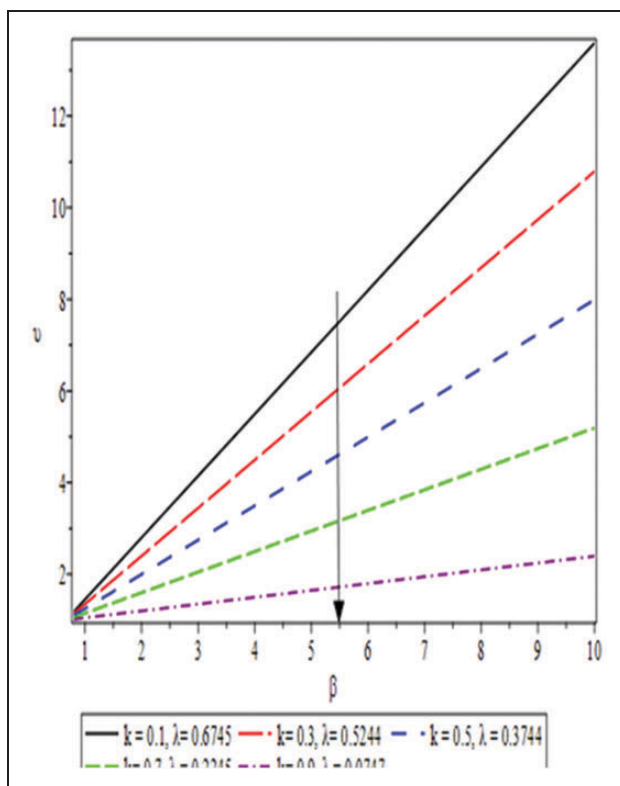


Figure 22. Impact of k on coating thickness.

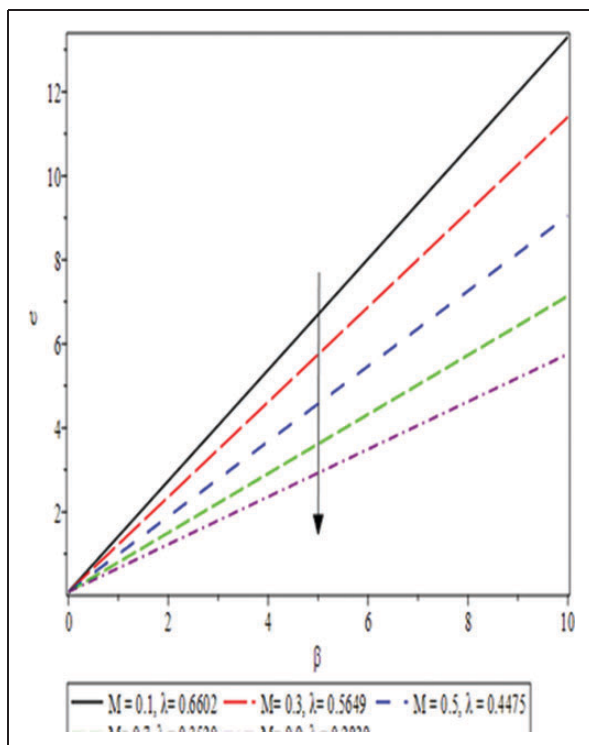


Figure 23. Impact of M on coating thickness.

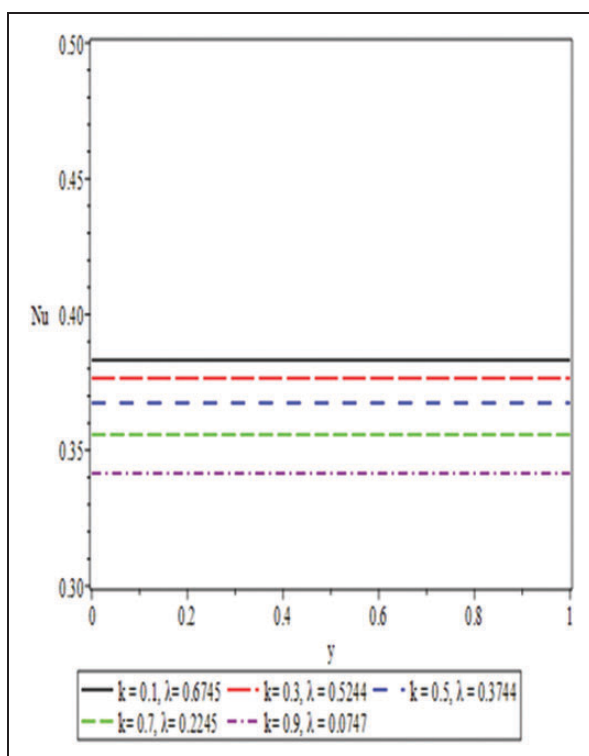


Figure 24. Effect of velocities ratio k on Nusselt Number.

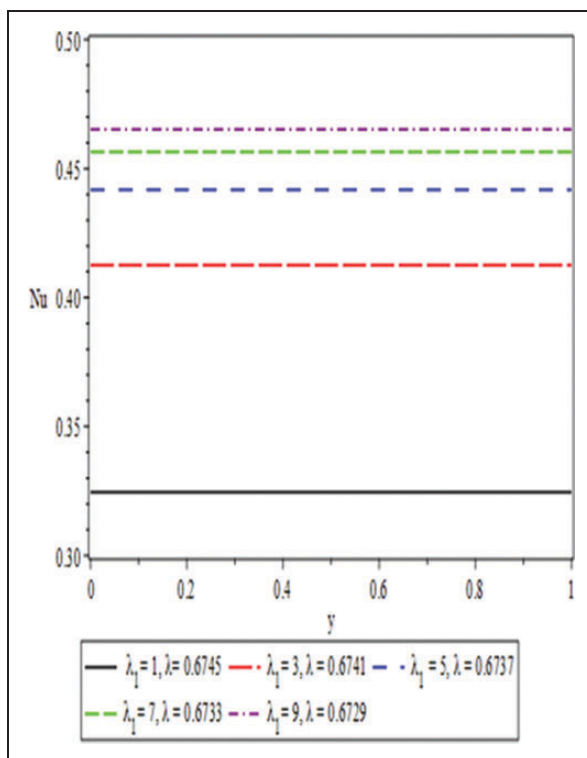


Figure 25. Effect of Jeffrey parameter λ_1 on Nusselt Number.

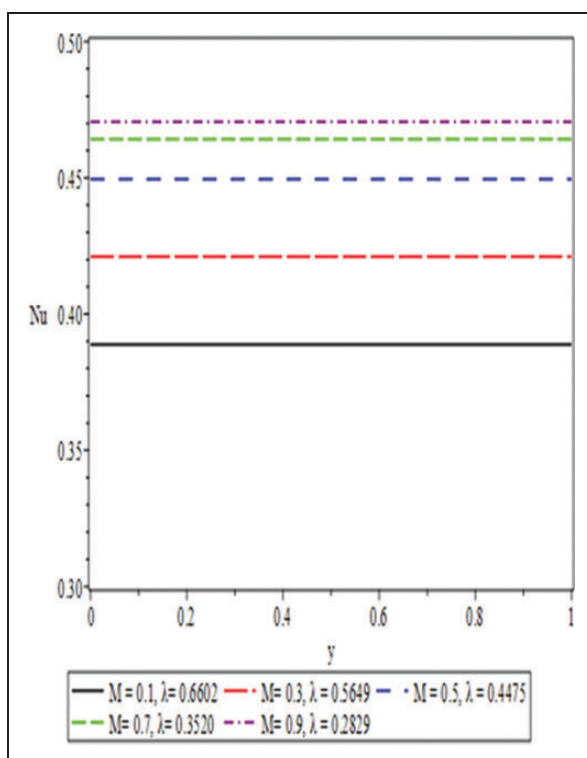


Figure 26. Effect of MHD M on Nusselt Number.

Results and discussion

The theoretical assessment of viscoelastic (Jeffrey) fluid for reverse roll coating has been examined. The Maple-19 has been used to obtain graphs and numerical solutions of this work. LAT is utilized to simplify the governing equations. Analytical solutions for velocity distribution, pressure gradient, separation force, flow rate, power input, Nusselt number and temperature distribution are presented. The numeric results for separation points x_{sp} , flow rate λ , power input p_w , coating thickness v and roll separation force F for various velocities ratios k , Jeffrey fluid parameter λ_1 and MHD parameter M are in Tables 1 to 4. One sees in Tables 1 to 3 that the coating thickness, separation points and flow rate decrease for increasing k , M and λ_1 . Also, the magnitude of power input increases, whereas k increases, the magnitude of roll separation force decreases. We found that when $\lambda_1 \rightarrow 0$ and $M \rightarrow 0$ the Newtonian results¹² are reproduced (Table 5). For different $\beta = \frac{H_0}{H_r}$, setting $k = 0.1$, $M = 0.3$ and $\lambda_1 = 8$, the numerical results in Table 4 were generated. It is important to remember that by increasing the nip gap, the coating thickness v increases, on the other hand, the web coating decreases with increased velocity ratio.

Figures 2 to 7 present the dimensionless velocity profiles for several k , M and λ_1 at position $x = 0.0$ and 0.75 . The velocity in the Figure 2 has been sketched at the nip region ($x = 0$) for the various values of velocities ratio k in the domain $[0.1, 0.9]$. The velocity profile has been found to decrease when the values of k are increased. The highest velocity was observed on the reverse roll surface. Then it begins to decrease when moving in the direction of the forward roll and reaches to zero while $y \in [-0.002, 0.916]$, beyond this domain, depending on the value of k , the flow in the reverse way can be observed towards the web of coating. It is noted from Figure 3 that at different positions in the procedure of reverse roll coating, when moving in the direction of the separation point, the domain of y , where the velocity reaches to zero increases, after this domain depending upon the values of k , the magnitude of the velocity increases when travelling in the direction of the upper roll and reaches to its maximum value on the surface of the roll. Here it is noted that compatibility with the model's predictions is reasonably appropriate for small k , whereas for larger k compared to unity, deviation increases. The Figures 4 to 7 show the velocity outcomes for the numerous values of M and λ_1 at distinct points ($x = 0, 0.75$) in the process of reverse roll coating. It has been seen from these graphs that the fluid velocity reduces by increasing M and λ_1 .

The graphical results for pressure gradient $\frac{dp}{dx}$ versus the axial coordinate x for the involved parameter k (velocities ratio) M (MHD parameter) and λ_1 (Jeffrey parameter) from 0.1 to 0.9 have been presented in Figures 8 to 10. It has been observed from these figures that the pressure gradients magnitude decreases for the increasing values of k , M and λ_1 . The dimensionless graphical depictions of pressure distributions for the numerous values of k , M and λ_1 are drawn in Figures 11 to 13. From Figures 11 to 13, it is witnessed that the pressure distributions magnitude increases by increasing the values of involved parameters like k , M and λ_1 .

It is witnessed from Figure 11 that the highest value of the pressure distributions magnitude occurs in the interval (0.1,0.2). Similar trend can be observed from Figures 12 and 14.

The influence of different parameters such as M , λ_1 , k and Brickman number Br on non-dimension temperature profile have been sketched in Figures 14 to 21 at different positions during reverse roll coating process. Figures 14 and 15 are drawn at $x = 0$ and $x = 0.75$ for increasing values of k whereas the M , λ_1 and Br are kept fixed. From Figures 16 to 19 it has been observed that for increasing value of M and λ_1 the temperature profile decreases. Whereas the converse behavior has been observed for the increasing value of k and Br .

The Figures 22 and 23 presents the graphical presentations of coating thickness for numerous values of parameters k and M . One can witness that the thickness of coating is decreasing function of k and M . The effect of the velocities ratio, Jeffrey parameter and MHD on the Nusselt numbers are explored in Figures 24 to 26. The values of Nusselt numbers are maximum for Jeffrey parameter and MHD, whereas opposite behaviors has been observed for velocities ratio.

Conclusions

The theoretical assessment of coating process during reverse roll for an incompressible, MHD, non-isothermal Jeffrey fluid is presented. The analytical solutions for velocity profile, temperature distribution and pressure gradients are found. The flow rate, coating thickness, separation points, pressure distributions, power input and force of roll separation are tabulated in numerical form.

The key deductions from this analysis are as follows:

- The maximum coating thickness 1.3141 was for velocities ratio $k = 0.1$, and the minimum coating thickness 1.0344 was at $k = 0.9$.
- The coating thickness to the maximum can be as high as 1.3142 versus the separation point is 0.99998 for $\lambda_1 = 1$, and the minimum coating thickness 1.3113 has been observed for $\lambda_1 = 9$.
- For increasing relaxation time divided by retardation time (λ_1), the magnitude of roll separation force and power input decrease.
- The velocities of the flow and pressure gradient decrease as λ_1 increases.
- The highest velocity occurs on the reverse roll surface.
- At the nip point, the absolute pressure gradient is maximum.
- Jeffrey fluid parameter (λ_1) plays an important role in controlling the pressure gradients.
- The pressure distribution increases as λ_1 and k increases
- The temperature profile decreases with M and λ_1 , and increases with k and Br .
- λ_1 provides an economical way to control the velocity, flow rate and web coating thickness.
- If $\lambda_1 \rightarrow 0$, $M \rightarrow 0$ the Newtonian results ¹² (Table 5) are reproduced.

Future scope

Engineers and scientists of related industries from all over the world are welcomed to validate our results in a real environment on an experimental basis. Our study mainly emphasized the theoretical analysis of viscoelastic materials.

Declaration of conflicting interests


The author(s) declared no potential conflicts of interest with respect to the research, authorship, and/or publication of this article.

Funding

The author(s) disclosed receipt of the following financial support for the research, authorship, and/or publication of this article: This research article is funded by Natural Science Foundation of China (NSFC), grant number 11971378.

ORCID iDs

Fateh Ali  <https://orcid.org/0000-0003-4755-8370>

Muhammad Zahid  <https://orcid.org/0000-0002-5136-2621>

References

1. Balzarotti F and Rosen M. Systematic study of coating systems with two rotating rolls. *Latin Am Appl Res* 2009; 39: 99–104.
2. Belblidia F, Tamaddon-Jahromi HR, Echendu SOS, et al. Reverse roll-coating flow: a computational investigation towards high-speed defect free coating. *Mech Time-Depend Mater* 2013; 17: 557–579.
3. Zheng G, Wachter F, Al-Zoubi A, et al. Computations of coating windows for reverse roll coating of liquid films. *J Coat Technol Res* 2020; 17: 897–910.
4. Abbas Z and Khaliq S. Calendering analysis of non-isothermal viscous nanofluid containing Cu-water nanoparticles using two co-rotating rolls. *J Plastic Film Sheet* 2021; 37: 182–204.
5. Abbas Z and Khaliq S. Roll-over-web coating analysis of micropolar-Casson fluid: a theoretical investigation. *J Polym Eng* 2021; 41: 289–298.
6. Khaliq S and Abbas Z. Analysis of calendering process of non-isothermal flow of non-Newtonian fluid: a perturbative and numerical study. *J Plastic Film Sheet* 2021. DOI:10.1177/8756087920979024.
7. Benkreira H, Edwards MF and Wilkinson WL. A semi-empirical model of the forward roll coating flow of Newtonian fluids. *Chem Eng Sci* 1981; 36: 423–427.
8. Greener J and Middleman S. Theoretical and experimental studies of the fluid dynamics of a two-roll coater. *Ind Eng Chem Fund* 1979; 18: 35–41.
9. Zafar M, Rana MA, Zahid M and Ahmad B. Mathematical analysis of the coating process over a porous web lubricated with upper-convected Maxwell fluid. *Coatings* 2019; 9: 458.
10. Zahid M, Zafar M, Rana MA, et al. Numerical analysis of the forward roll coating of a Rabinowitsch fluid. *J Plastic Film Sheet*. DOI: 10.1177/08756087919887216.
11. Pitts E and Greiller J. The flow of thin liquid films between rollers. *J Fluid Mech* 1961; 11: 33–50.

12. Greener J and Middleman S. Reverse roll coating of viscous and viscoelastic liquids. *Ind Eng Chem Fund* 1981; 20: 63–66.
13. Ho WS and Holland FA. Between-rolls metering coating technique. A theoretical and experimental study. *TAPPI* 1978; 61: 53–56.
14. Coyle DJ, Macosko CW and Scriven LE. The fluid dynamics of reverse roll coating. *AIChE J* 1990; 36: 161–174.
15. Hao Y and Haber S. Reverse roll coating flow. *Int J Numer Meth Fluids* 1999; 30: 635–652.
16. Taylor J and Zettlemoyer A. Hypothesis on the mechanism of ink splitting during printing. *Tappi J* 1958; 12: 749–757.
17. Hintermaier J and White R. The splitting of a water film between rotating rolls. *Tappi J* 1965; 48: 617–625.
18. Ali F, Hou Y, Zahid M, et al. Theoretical study of the reverse roll coating of non-isothermal magnetohydrodynamics viscoplastic fluid. *Coatings* 2020; 10: 940.
19. Ali F, Hou Y, Zahid M, et al. Mathematical analysis of pseudoplastic polymers during reverse roll-coating. *Polymers* 2020; 12: 2285.
20. Farooqi A, Ahmad R, Alotaibi H, et al. A comparative epidemiological stability analysis of predictor corrector type non-standard finite difference scheme for the transmissibility of measles. *Results Phys* 2021; 21: 103756.
21. Farooqi A, Ahmad R, Farooqi R, et al. An accurate Predictor-Corrector-Type nonstandard finite difference scheme for an SEIR epidemic model. *J Math* 2020; 2020: 1–18.
22. Sofou S and Mitsoulis E. Roll-over-web coating of pseudoplastic and viscoplastic sheets using the lubrication approximation. *J Plastic Film Sheet* 2005; 21: 307–333.
23. Ahmad R, Farooqi A, Zhang J, et al. Steady flow of a power law fluid through a tapered non-symmetric stenotic tube. *Appl Math Nonlin Sci* 2019; 4: 255–266.
24. Nadeem S and Akram S. Peristaltic flow of a Jeffrey fluid in a rectangular duct. *Nonlin Anal: Real World Appl* 2010; 11: 4238–4247.
25. Srinivas S and Muthuraj R. Peristaltic transport of a jeffrey fluid under the effect of slip in an inclined asymmetric channel. *Int J Appl Mechanics* 2010; 02: 437–455.
26. Hayat T, Awais M, Alsaedi A, et al. 3-D flow of Jeffery fluid in a channel with stretched wall. *Eur Phys J Plus* 2012; 127: 128.
27. Turkiymazoglu M. Numerical and analytical solutions for the flow and heat transfer near the equator of an MHD boundary layer over a porous rotating sphere. *Int J Thermal Sci* 2011; 50: 831–842.
28. Bhattacharyya K and Pop I. MHD boundary layer flow due to an exponentially shrinking sheet. *Magnetohydrodynamics* 2011; 47: 337–344.
29. Makinde O. Computational modelling of MHD unsteady flow and heat transfer toward a flat plate with Navier slip and Newtonian heating. *Braz J Chem Eng* 2012; 29: 159–166.
30. Ramesh K, editor Influence of heat transfer on poiseuille flow of MHD Jeffrey fluid through porous medium with slip boundary conditions. In: *AIP conference proceedings*, 1860, 020044 (2017). AIP Publishing LLC. DOI: 10.1063/1.4990343.
31. Shercliff JA. *Textbook of magnetohydrodynamics*. 1965.
32. Khaliq S and Abbas Z. A theoretical analysis of roll-over-web coating assessment of viscous nanofluid containing Cu-water nanoparticles. *J Plastic Film Sheet* 2020; 36: 55–75.

Biographies

Fateh Ali is a PhD scholar in the School of Mathematics & Statistics, Xi'an Jiaotong University, Shaanxi, Xi'an, China. His research interest is Fluid Mechanics, Nonlinear Analysis, Roll Coating and Numerical Methods.

Yanren Hou is a professor of Mathematics in the School of Mathematics & Statistics, Xi'an Jiaotong University, Shaanxi, Xi'an, China. His research interest is Numerical Methods for PDEs, Navier-Stoke Equations, Numerical Analysis.

Muhammad Zahid is an assistant professor of Mathematics in the Department of Mathematics, COMSATS University Islamabad, Abbottabad Campus, Abbottabad, Pakistan. His research Interest is Fluid Mechanics, Calendering Coating Analysis, Nonlinear Analysis, Numerical Methods, Perturbation Methods.

MA Rana is a professor of Mathematics in the Department of Mathematics & Statistics, Riphah International University Islamabad, Pakistan. His research interest is Fluid Mechanics, Nonlinear Analysis, Mathematical Modelling and Numerical Methods

Muhammad Usman is a PhD scholar in the School of Mathematics & Statistics, Xi'an Jiaotong University, Shaanxi, Xi'an, China. His research interest is Fluid Mechanics, Nonlinear Analysis and Numerical Methods.

Appendix

Notation

Br	Brickman number
$C_p \left(\frac{J}{Kg.K} \right)$	specific Heat capacity
$J \left(\frac{ampere}{m^2} \right)$	current density
$H_f (m)$	the thickness of the coating on the forwarding roll
$H_r (m)$	the thickness of the coating on reverse roll
H_0	half of the nip separation
$k \frac{U_r}{U_f}$	velocities ratio
$R (m)$	the radius of each roll
T	extra stress tensor
$U_f \left(\frac{m}{s} \right)$	peripheral velocity of forwarding roll
$U_r \left(\frac{m}{s} \right)$	peripheral velocity of the reverse roll
$\beta \frac{H_0}{H_r}$	ratio of the half of the nip separation to the coating thickness on the reverse roll

λ	dimensionless flow rate
λ_1 (s)	Jeffrey fluid parameter
$\rho \left(\frac{\text{kg}}{\text{m}^3} \right)$	fluid density
$v \frac{H_f}{H_r}$	coating thickness